Chemical Speciation & Bioavailability

ISSN: 0954-2299 (Print) 2047-6523 (Online) Journal homepage: https://www.tandfonline.com/loi/tcsb20

Pyrogenic temperature affects the particle size of biochar-supported nanoscaled zero valent iron (nZVI) and its silver removal capacity

Shengsen Wang, Mingyue Zhao, Yiting Zhao, Nong Wang, Jing Bai, Ke Feng, Yanxia Zhou, Wangshu Chen, Fangfang Wen, Saisai Wang, Xiaozhi Wang & Jun Wang

To cite this article: Shengsen Wang, Mingyue Zhao, Yiting Zhao, Nong Wang, Jing Bai, Ke Feng, Yanxia Zhou, Wangshu Chen, Fangfang Wen, Saisai Wang, Xiaozhi Wang & Jun Wang (2017) Pyrogenic temperature affects the particle size of biochar-supported nanoscaled zero valent iron (nZVI) and its silver removal capacity, Chemical Speciation & Bioavailability, 29:1, 179-185, DOI: 10.1080/09542299.2017.1395712

To link to this article: https://doi.org/10.1080/09542299.2017.1395712

Published online: 31 Oct 2017.

CHEMICAL SPECIATION & BIOAVAILABILITY, 2017
VOL. 29, NO. 1, 179–185
https://doi.org/10.1080/09542299.2017.1395712

Taylor & Francis
Taylor & Francis Group

Pyrogenic temperature affects the particle size of biochar-supported nanoscaled zero valent iron (nZVI) and its silver removal capacity

Shengsen Wang[a,b], Mingyue Zhao[b], Yiting Zhao[b], Nong Wang[c], Jing Bai[d], Ke Feng[b], Yanxia Zhou[b], Wangshu Chen[b], Fangfang Wen[b], Saisai Wang[b], Xiaozhi Wang[b] and Jun Wang[e]

[a]Ministry of Agriculture/Tianjin Key Laboratory of Agro-environment and Safe-product, Tianjin, China; [b]College of Environmental Science and Engineering, Yangzhou University, Yangzhou, China; [c]Agro-environmental Protection Institute, Ministry of Agriculture of the People's Republic of China, Tianjin, China; [d]Institute of Modern Physics, Chinese Academy of Sciences, Lanzhou, China; [e]College of Resources and Environment, Key Laboratory of Agricultural Environment in Universities of Shandong, Shandong Agricultural University, Taian, PR China

ABSTRACT

Particle size of nanoscaled zero valent iron (nZVI) in nanocomposites can be affected by support materials. In this work, nZVI was supported by bamboo-derived biochars produced at 450 °C (BBL) and 600 °C (BBH). Total iron (Fe) contents were 14.4 and 11.9% for nZVI immobilized in BBL (nZVI/BBL) and BBH (nZVI/BBH), respectively. The resultant nanocomposites were characterized by transmission electron microscopy (TEM), X-ray diffraction (XRD), and scanning electron microscopy/energy-dispersive X-ray analyses (SEM/EDS). The nZVI was successfully embedded in biochar pores and surfaces as confirmed by SEM/EDS and XRD. TEM revealed that particle sizes of nZVI in nZVI/BBL and nZVI/BBH were roughly 26 and 40 nm, respectively. The Ag^+ sorption isotherms (25–300 mg L^{-1} Ag^+) suggested that 1 kg of nZVI in nZVI/BBL and nZVI/BBH removed as much as 745.5 and 534.5 g Ag^+, respectively. The results suggested that Ag^+ removal capacity was related to particle size of nZVI, which was also affected by pyrogenic temperature.

ARTICLE HISTORY
Received 9 July 2017
Accepted 17 October 2017

KEYWORDS
Zero valent iron; pyrogenic temperature; particle size; biochar; silver ion; reduction

1. Introduction

Recently, nanoscaled zero valent iron (nZVI) has been extended for *in situ* remediation of reducible heavy metals [1]. The importance of the dimension of nanoparticles (NPs) on heavy metal removal was highlighted in many previous work [2]. Small particle size endows unique properties of NPs. For example, sorptive removal of heavy metals by maghemite (γ-Fe_2O_3) was enhanced as the particle size decreased, which was ascribed to large surface area and favorable atomic structure and surface free energies [3]. It is presumably true that the properties of nZVI may also be size-dependent, e.g. nZVI became super-paramagnetic as its size was reduced to 5 nm [4]. Thus, it is very important to manipulate the dimension of NPs for environmental remediation.

However, high tendency of agglomeration of NPs could increase the particle size and reduce reactivity of nZVI. Previous work prepared nanoparticles by using such surfactant or stabilizer as carboxymethyl cellulose (CMC) [5], poly(acrylic acid) (PAA) [6] and polyvinyl-alcohol (PVA) [7]. However, the use of these organic surfactant tends to alter the sorptive and reductive performance of nanoparticles (unpublished work). Instead, nZVI can be stabilized by porous supporting matrix, e.g. carbonaceous matrix (graphene, resins, carbon nanotubes) [1,8,9] and silicate minerals (zeolite, montmorillonite) [10,11].

Biochar is a common support matrix for NP immobilization [12,13]. The biochar supported nZVI are characterized with smaller and stabilized particle size with enhanced heavy metal removal capacity [11]. The dimension of nZVI NP appeared to be related with biochar properties, e.g. grain size of nZVI was 25.3 nm [14] and 2 nm [12] in different biochar matrix. Thus, properties of biochar could affect dispersion and formation of the nZVI NPs [4]. Our recent work indicated that biochar pore characteristics are related to crystallite size of nZVI [15]. It is well documented that increased temperatures can reduce pore size [16,17], functional groups [18], and increase pH [19] of biochars. However, few studies have investigated the averaged particle size of nZVI in relation to biochar property. Thus, a comparative study was undertaken to understand the effects of pyrogenic temperature of biochars on particle size of nZVI.

Unlike maghemite, nZVI is composed of metallic iron entrapped with iron oxides, which exhibits both sorptive and reductive capacity for environmental contaminants. However, the sorptive and reductive capacity of nZVI has been seldom investigated in relation to particle size. Thus,

CONTACT Jun Wang jwang@sdau.edu.cn

the present study also examined the reductive capacity of nZVI of different particle size. Although Ag^+ has been used in past decades for medication purpose, excessive Ag^+ is hazardous to living organisms [20]. Metallic Ag nanoparticles (AgNP) are highly dynamic in the aquatic system, and demonstrate more favorable properties [21]. However, wide use of Ag nanoparticles (AgNP) in soil and water may enhance Ag^+ release and accumulation into environment, which is responsive to environmental factors. For example, previous work demonstrated that sunlight density facilitates AgNP aggregation in aquatic system, while dissolved organic matter tends to stabilize AgNPs [22]. The analysis of AgNPs is favored by a preconcentration technique, i.e. cloud point extraction, proposed by Liu et al. [23]. To alleviate environmental hazard, Ag^+ reduction to metallic Ag (Ag^0) is often achieved by some facile routes, i.e. biomass [24], biochars [25], and nZVI [26]. Thus, Ag^+ reduction capacity by nZVI was evaluated in this work.

To date, the effects of pyrogenic temperature of biochars on particle size of nZVI and its reductive capacity of Ag^+ have not been well established. In this work, the nZVI was supported by bamboo-derived biochars pyrolyzed at 450 and 600 °C. The resultant nZVI and biochar composites were characterized and examined for Ag^+ removal. The objectives of this study were to (1) investigate temperature effects on biochar properties in relation to particle size of nZVI, and (2) examine the Ag^+ removal capacity in response to particle size of biochar-supported nZVI.

2. Materials and methods

2.1. Reagents

All chemicals were dissolved with ultrapure water (Nanopure water, Barnstead) denoted as DI water (18.2 MΩ). Chemicals of analytical grade was used, including silver nitrate ($AgNO_3$), ferric chloride hexahydrate ($FeCl_3{\cdot}6H_2O$) and sodium borohydride ($NaBH_4$).

2.2. Biochar preparation and modification

Bamboo wood was oven dried at 80 °C and then pyrolyzed at 450 °C (BBL) and 600 °C (BBH) in a sealed kiln (MTI, Richmond, CA). The resulting biochars were crushed and rinsed with tap water for 1 h and DI water for 10 min, and oven dried overnight at 80 °C.

The biochar supported nZVI was prepared following our previous method [12]. Briefly, 4 g biochar was suspended in 270 ml DI water followed by sonication for 1 h. Meanwhile, $FeCl_3{\cdot}6H_2O$ was dissolved in 30 ml DI water, and resultant solution was mixed with biochar suspension, equivalent to 0.02 M $FeCl_3{\cdot}6H_2O$. Subsequently, 4 g $NaBH_4$ was dissolved in 50 ml DI water, and added dropwise to above solution to reduce Fe^{3+} to metallic Fe at 90 °C. The entire process was protected with purged argon gas to remove air from solutions. The suspension was vacuum filtered, and rinsed with DI water and ethanol, to obtain nZVI/BBL and nZVI/BBH composites.

2.3. Sorbent characterization

Specific surface area and pore volume were measured using a NOVA 1200 analyzer and calculated with density functional theory (DFT) theory. Total Fe content in supported nZVI was prepared with AOAC method (1990). Both Fe and Ag^+ were analyzed with an inductively coupled plasma-atomic emission spectrometry (ICP-AES, Perkin-Elmer Plasma 3200). Surface morphology and Fe distribution were visualized with a scanning electron microscope (SEM) (JEOL JSM-6400 Scanning Microscope) coupled with an Energy dispersive X-ray spectroscopy (EDS, Oxford Instruments Link ISIS). Both nZVI and metallic Ag were identified with a CuKα radiation X-ray diffractometer (XRD) (Ultima IV X-ray Diffractometer, Rigaku Corporation, Japan). The particle size of nZVI was obtained from a transmission electron microscopy (TEM) (Tecnai 12, Philips Electronic Instruments).

2.4. Ag^+ removal experiments

The batch sorption experiment was conducted at room temperature (22 ± 0.5 °C). For isotherm experiment,

Table 1. Major elemental composition and surface area of BBL, BBH, nZVI/BBL, and nZVI/BBH.

	C	N	Fe	CO_2 DFT surface area (SA)	DFT pore vol (des. leg)
	Mass (%)			$m^2\ g^{-1}$	$cc\ g^{-1}$
BBL	73.93	0.37	<0.02	328.1	0.091
BBH	83.70	0.36	<0.02	507.5	0.136
nZVI/BBL	65.30	0.31	14.4	302.1	0.084
nZVI/BBH	70.95	0.33	11.9	421.6	0.113

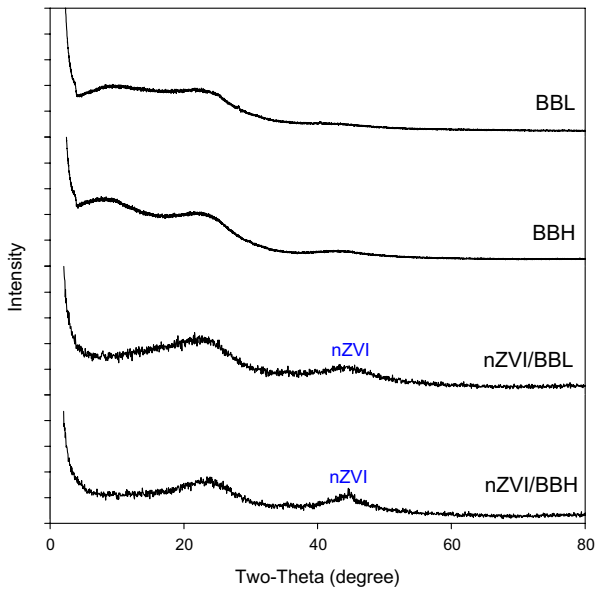

Figure 1. XRD diffraction patterns of BBL, BBH, nZVI/BBL and nZVI/BBH.

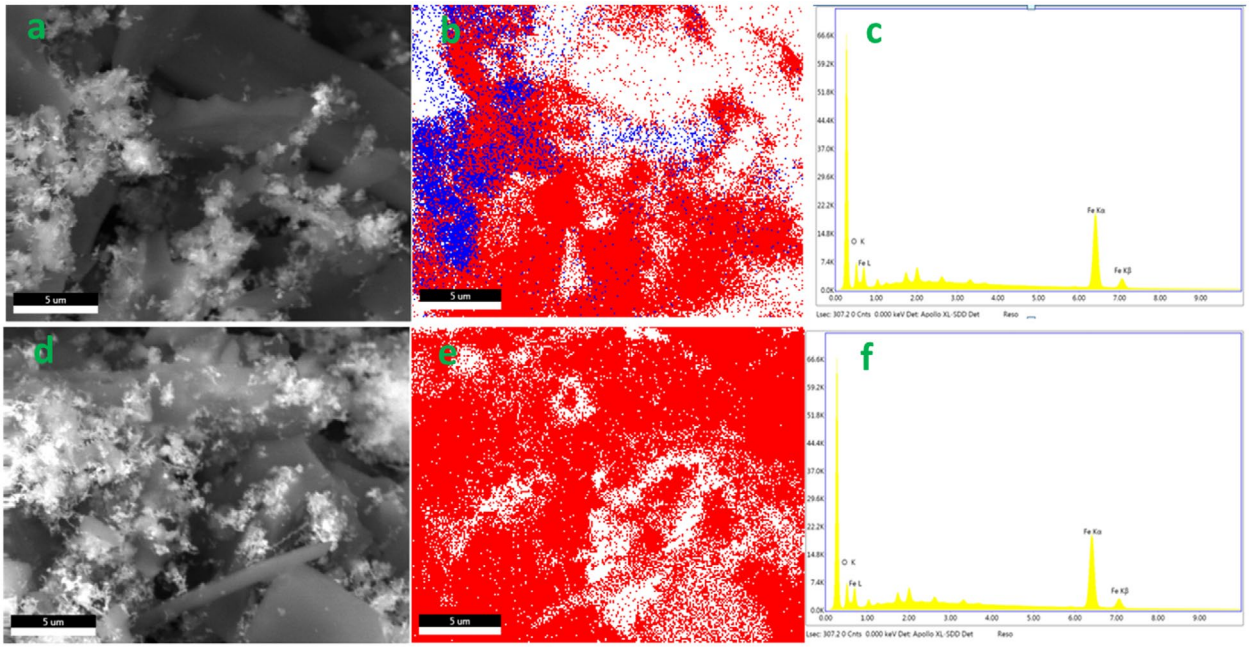

Figure 2. SEM topography (a, d), EDS elemental distribution map (b, e), and EDS spectra (c, f) of nZVI/BBL (a–c) and nZVI/BBH (d–f).

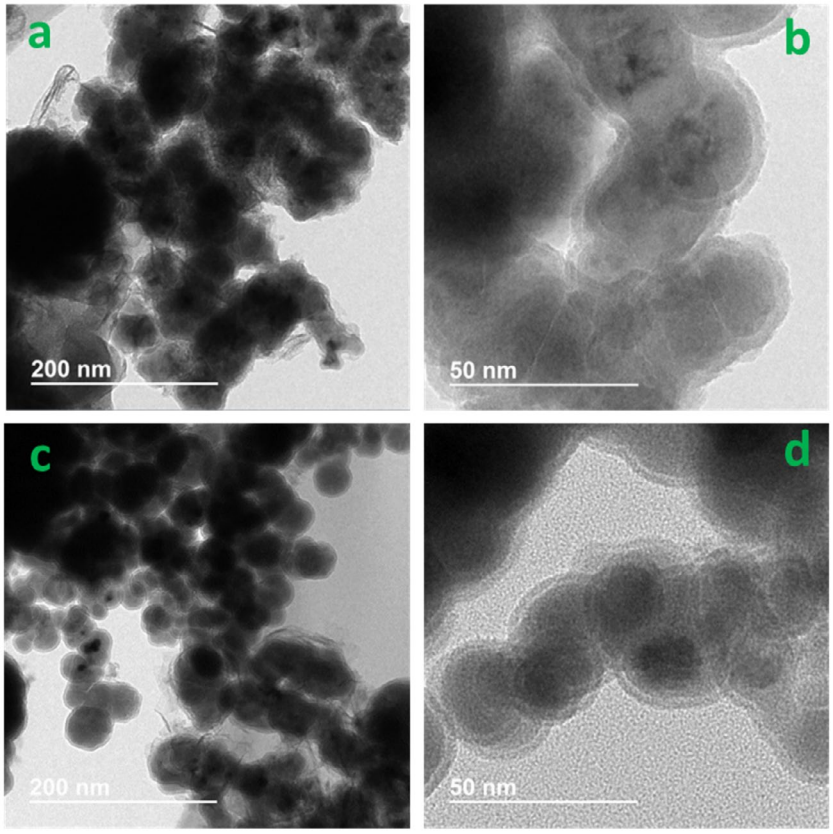

Figure 3. TEM with 25,000× (a, c) and 100,000× (b, d) magnification for nZVI/BBH (a, b) and nZVI/BBL (c, d).

0.04 g sorbents were either added to 20 mL (2 g L^{-1}) of 25, 50, 100, 200 and 300 mg L^{-1} Ag^{+} solution in 68 mL digestion vessels (Environmental Express). After 24 h reaction, the suspensions were immediately filtered through 0.22 µm pore size nylon membrane filters (GE cellulose nylon membrane). The spent sorbents were vacuum dried and the filtrate was analyzed with ICP. All treatments were triplicated and the means were reported with standard deviation.

Isotherm data were simulated with Langmuir isotherm models, and the governing equations can be written as follows [27]:

$$q_e = \frac{KS_{\max C_e}}{1 + KC_e}, \text{ Langmuir} \quad (1)$$

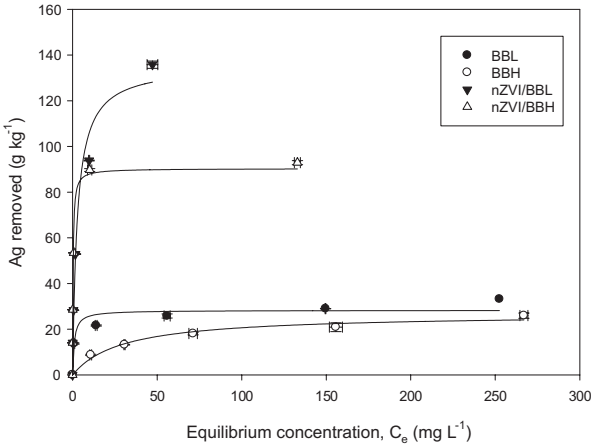

Figure 4. Ag^+ removal isotherm by BBL, BBH, nZVI/BBL and nZVI/BBH.

Table 2. Best-fit Langmuir model parameters for isotherms of Ag^+ removal by BBL, BBH, nZVI/BBL, and nZVI/BBH.

Biochar	S_{max} (g kg^{-1})	K (L g^{-1})	R^2
BBL	28.26	1.0134	0.9250
BBH	26.72	0.0339	0.9380
nZVI/BBL	135.61	0.3645	0.9700
nZVI/BBH	90.33	3.6749	0.9689

where K represents the Langmuir bonding term related to interaction energies (L g^{-1}), S_{max} is Langmuir maximum capacity (g kg^{-1}), C_e is Ag^+ concentration (g L^{-1}) at equilibrium.

3. Results and discussion

3.1. Characterization of sorbents

Higher pyrogenic temperature enhanced surface area (SA) and pore volume (PV) of biochars indicative of higher porosity. The SA and PV of BBH were 1.55 and 1.49 times that of BBL (Table 1). As expected, the impregnation of nZVI reduced both SA and PV of biochars because nZVI can both block pores and occupy the surface of porous biochars (Table 1).

The Fe in biochar matrix was also characterized for elemental composition, crystallinity and surface morphology. Total Fe contents in the nZVI and biochar composites were over 600 times greater than respective pristine biochars, and the low temperature char was able to accommodate more Fe (Table 1). Fe exists mainly as nZVI which was confirmed by XRD analysis, corresponding to the characteristic peaks at $2\theta = 44.5°$ (Figure 1) [28]. Wide nZVI peaks in composites may be attributed to low crystallinity or smaller grain size, suggesting nZVI/BBL has smaller nZVI than nZVI/BBH (Figure 1). No nZVI peaks appeared in pristine biochars, further confirming nZVI was successfully embedded in the nZVI/BBL and nZVI/BBH. The SEM surface morphology clearly revealed that nZVI particles were well

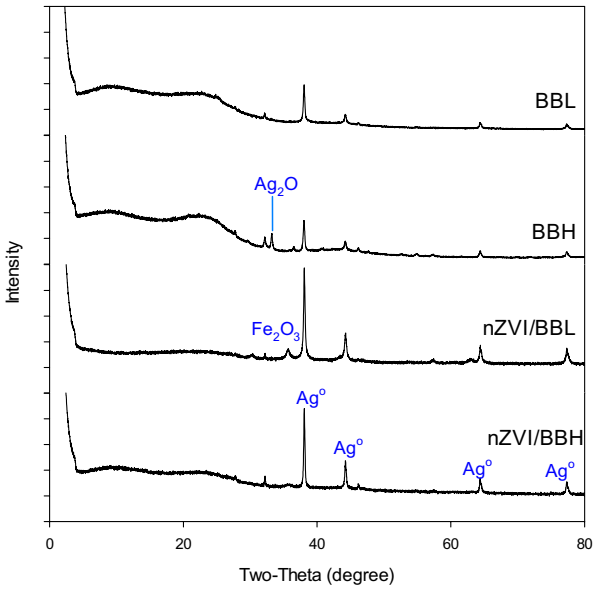

Figure 5. XRD diffraction patterns of Ag^+ spent BBL, BBH, nZVI/BBL and nZVI/BBH.

dispersed on biochar surface and pores, and Fe distribution was confirmed with EDS (Figure 2). More importantly, the nZVI particle size was different in biochars of different pyrogenic temperature. Both Debye-Scherrer equation [29] and TEM indicated that the grain size of nZVI was approximately 26 and 40 nm in diameter in nZVI/BBL and nZVI/BBH, respectively (Figure 3). This revealed that crystallite size of nZVI was affected by the pyrogenic temperature, perhaps attributing to different biochar properties.

3.2. Ag^+ removal by sorbents

The sorption data were well described by Langmuir isotherm model with coefficient of determination above 0.92 (Figure 4; Table 2). Compared to pristine biochars, the nZVI/biochar nanocomposites showed better fit of simulated curves as indicated by higher R^2. The disparity may be as the result of governing Ag^+ removal mechanisms. Since Langmuir model describes monolayer sorption and uniform reaction on the surface of the sorbents, it is likely that Ag^+ sorption by nZVI/biochar may be governed by more uniform reaction than pristine biochars. The maximum Ag^+ removal capacity was predicted by Langmuir model. Similar Ag^+ removal capacity occurred for two pristine biochars, whereas nZVI/BBL and nZVI/BBH greatly increased Ag^+ removal by 4.8 and 3.4 times relative to BBL and BBH, respectively. Apparently, the bulk nZVI/BBL removed more Ag^+ than nZVI/BBH by 1.5 times. Ag^+ removal capacity by pure nZVI suggested that nZVI/BBL and nZVI/BBH could remove as much as 745.5 and 534.5 g Ag^+ per kg of metallic Fe. Thus, BBL supported nZVI appeared to facilitate Ag^+ removal with greater Ag^+ removal capacity on both bulk sorbent and nZVI basis.

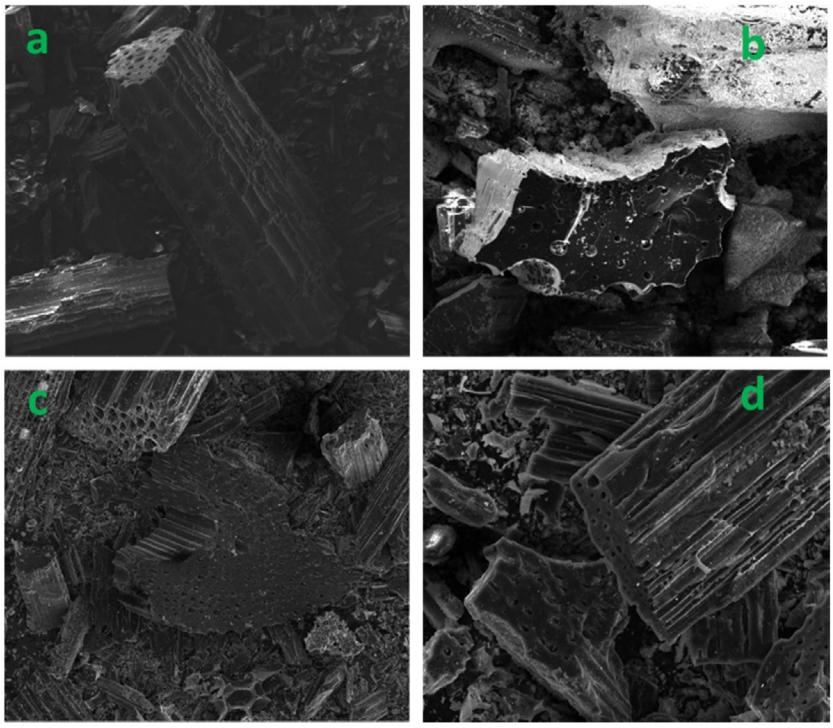

Figure 6. SEM of Ag^+ spent BBL (a), nZVI/BBL (b), BBH (c) and nZVI/BBH (d).

3.3. Pyrogenic temperature in relation to particle size and Ag^+ removal of nZVI

The nanoparticles demonstrate nanoscale effects, i.e. the sorptive and reductive properties are enhanced as the particle size decreases [30]. The sorptive capacity of different-sized nanoscaled Fe oxides has been well understood [3]. For example, the elevated sorptive removal capacity by smaller particles may be related to larger surface area and more favorable surface properties, i.e. re-arranged atom structure [31]. However, both sorptive and reductive capacity of nZVI of different particle size has yet been fully illustrated.

Several mechanisms may participate in Ag^+ removal. XRD diffractogram showed the characteristic peaks of metallic Ag at $2\theta = 38.16, 44.19, 64.51, 77.38°$ (Figure 5) for Ag spent biochars and biochar-supported nZVI. This showed that reduction was involved for Ag^+ removal for pristine biochars and nZVI/biochar composite. The abundant functional groups in biochar can accept or donate electrons [25,32,33], which can donate electrons for Ag^+ reduction. Similarly, nZVI is a more powerful electron donor to reduce Ag^+[26]. Isotherm model suggested that Ag^+ may be removed by mechanisms other than reduction for pristine biochars. For example, XRD results indicate Ag_2O appeared in Ag-spent biochars (Figure 5), which was also evidenced by a previous work by Yao et al. [25]. As compared to pristine biochars, excess Ag^+ removal by nZVI nanocomposites relative to pristine biochars was attributed to nZVI in the nanocomposites. Relative to nZVI in nZVI/BBH composites, nZVI in nZVI/BBL was even more reactive in Ag^+ removal. The greater Ag^+ removal by nZVI/BBL can also be visualized by white coating of Ag^o crystals on surface of sorbents (Figure 6(b)). The extraordinary reduction capacity of pure nZVI in support matrix suggested that smaller sized nZVI showed enhanced Ag^+ removal capacity. That is, the reduction of Ag^+ was facilitated by smaller-sized nZVI.

Since same protocol was adopted to synthesize nZVI in two biochars, the varied particle size should result from difference in biochar properties [15]. In this work, pyrogenic temperature was selected as the sole variable, because a number of work demonstrated that biochar properties are closely related to pyrolysis temperature. For example, biochars produced at 600 °C may be characterized as smaller pore opening, less functional groups and higher pH relative to that at 450 °C [17]. Previous work has demonstrated that formation of nZVI was heavily dependent onto environmental conditions [34]. Thus, nZVI particle size may be manipulated by biochar properties largely dependent on temperature for specific feedstock. SEM images indicate nZVI can be partially trapped in pores, and thus pore opening may affect the size of nanoscaled particles. However, some other properties of biochars may also contribute to difference in particle size of nZVI. Therefore, additional work is needed to discriminate the contribution of different biochar properties on nZVI particles size. Moreover, the aggregation of nZVI can complicate identification of possible influencing factors. Thus, it may be helpful to separate the nZVI clusters on biochar surfaces.

4. Conclusions

In this work, bamboo biomass was pyrolyzed at both 450 and 600 °C, and resultant biochars were used to support nZVI. The averaged nZVI crystallite size for nZVI/BBL (26 nm) was smaller than nZVI/BBH (40 nm). XRD confirmed that Ag^+ was dominantly reduced to Ag^o by both biochars and biochar supported nZVI. The Ag^+ removal by nZVI/BBL was 1.5 times greater than nZVI/BBH, and Ag^+ removal by nZVI (745.5 g kg^{-1} nZVI) in nZVI/BBL was greater than nZVI (534.5 g kg^{-1} nZVI) in nZVI/BBH. That is, Ag^+ removal capacity was negatively related to particle size of nZVI, which was affected by pyrogenic temperature. However, detailed work is needed to identify the potential effects of biochar properties on particle size of nZVI.

Disclosure statement

No potential conflict of interest was reported by the authors.

Funding

This research was supported by National Science Foundation of China [grant number 41771349]; Open Fund of Key Laboratory of Key Laboratory of Original Agro-Environmental Pollution Prevention and Control/Ministry of Agriculture/Tianjin Key Laboratory of Agro-environment and Safe-product (2017); Startup Fund for distinguished scholars of Yangzhou University [grant number 5016/137011014]; Social Development Program of Jiangsu Province, China [grant number BE2015661]; Independent Innovation Project of Jiangsu Province [grant number CX(12)1001-06]; Six Talent Peaks Project of Jiangsu Province, China [grant number 2013-NY-017].

References

[1] Ponder SM, Darab JG, Mallouk TE. Remediation of Cr(VI) and Pb(II) aqueous solutions using supported, nanoscale zero-valent iron. Environ Sci Technol. 2000;34:2564–2569.
[2] Carlos L, Einschlag FSGa, González MnC, Mártire DO, Applications of magnetite nanoparticles for heavy metal removal from wastewater. In: Einschlag FSGa, Carlos L., editors. Waste water – treatment technologies and recent analytical developments. Rijeka: InTech; 2013. Ch. 03.
[3] Auffan M, Rose J, Proux O, et al. Enhanced adsorption of arsenic onto maghemites nanoparticles: As(III) as a probe of the surface structure and heterogeneity. Langmuir. 2008;24:3215–3222.
[4] Tuček J, Sofer Z, Bouša D, et al. Air-stable superparamagnetic metal nanoparticles entrapped in graphene oxide matrix. Nat Commun. 2016;7:12879.
[5] Hashem M, Sharaf S, Abd El-Hady MM, et al. Synthesis and characterization of novel carboxymethylcellulose hydrogels and carboxymethylcellulolse-hydrogel-ZnO-nanocomposites. Carbohydr Polym. 2013;95:421–427.
[6] Cushing BL, Kolesnichenko VL, O'Connor CJ. Recent advances in the liquid-phase syntheses of inorganic nanoparticles. Chem Rev. 2004;104:3893–3946.
[7] Qin L, Shing C, Sawyer S, et al. Enhanced ultraviolet sensitivity of zinc oxide nanoparticle photoconductors by surface passivation. Opt. Mater. 2011;33:359–362.
[8] Jabeen H, Chandra V, Jung S, et al. Enhanced Cr(vi) removal using iron nanoparticle decorated graphene. Nanoscale. 2011;3:3583–3585.
[9] Lv X, Xu J, Jiang G, et al. Removal of chromium(VI) from wastewater by nanoscale zero-valent iron particles supported on multiwalled carbon nanotubes. Chemosphere. 2011;85:1204–1209.
[10] Kim SA, Kamala-Kannan S, Lee KJ, et al. Removal of Pb(II) from aqueous solution by a zeolite–nanoscale zero-valent iron composite. Chem Eng J. 2013;217:54–60.
[11] Bhowmick S, Chakraborty S, Mondal P, et al. Montmorillonite-supported nanoscale zero-valent iron for removal of arsenic from aqueous solution: Kinetics and mechanism. Chem Eng J. 2014;243:14–23.
[12] Wang S, Gao B, Li Y, et al. Adsorptive removal of arsenate from aqueous solutions by biochar supported zero-valent iron nanocomposite: Batch and continuous flow tests. J Hazard Mater. 2016;322:172–181.
[13] Wang S, Gao B, Li Y, et al. Manganese oxide-modified biochars: preparation, characterization, and sorption of arsenate and lead. Bioresour Technol. 2015;181:13–17.
[14] Yan J, Han L, Gao W, et al. Biochar supported nanoscale zerovalent iron composite used as persulfate activator for removing trichloroethylene. Bioresour Technol. 2014;175:269–274.
[15] Wang S, Zhou Y, Gao B, et al. The sorptive and reductive capacities of biochar supported nanoscaled zero-valent iron (nZVI) in relation to its crystallite size. Chemosphere. 2017;186:495–500.
[16] Baltrėnas P, Baltrėnaitė E, Spudulis E. Biochar from pine and birch morphology and pore structure change by treatment in biofilter. Water Air Soil Pollut. 2015;226:1–14.
[17] Yakout SM, Daifullah AEHM, El-Reefy SA. Pore structure characterization of chemically modified biochar derived from rice straw. Environ Eng Manage J. 2015;14:473–480.
[18] Keiluweit M, Nico PS, Johnson MG, et al. Dynamic molecular structure of plant biomass-derived black carbon (biochar). Environ Sci Technol. 2010;44:1247–1253.
[19] Wang S, Gao B, Zimmerman AR, et al. Physicochemical and sorptive properties of biochars derived from woody and herbaceous biomass. Chemosphere. 2015;134:257.
[20] Yu S, Liu J. Introduction. In: Liu J, Jiang G, editors. Silver nanoparticles in the environment. Berlin, Heidelberg: Springer Berlin Heidelberg; 2015. p. 1–8.
[21] Yu SJ, Yin YG, Liu JF. Silver nanoparticles in the environment. Environ Sci Processes Impacts. 2013;15:78.
[22] Yu S, Yin Y, Chao J, et al. Highly dynamic PVP-coated silver nanoparticles in aquatic environments: chemical and morphology change induced by oxidation of Ag 0 and reduction of Ag +. Environ Sci Technol. 2014;48:403–411.
[23] Liu JF, Chao JB, Liu R, et al. Cloud point extraction as an advantageous preconcentration approach for analysis of trace silver nanoparticles in environmental waters. Anal Chem. 2009;81:6496–6502.
[24] Jyoti K, Baunthiyal M, Singh A. Characterization of silver nanoparticles synthesized using Urtica dioica Linn. leaves and their synergistic effects with antibiotics. J Radiat Res Appl Sci 2016; 9:217–227.
[25] Yao Y, Gao B, Wu F, et al. Engineered biochar from biofuel residue: characterization and its silver removal potential. ACS Appl Mater Interfaces. 2015;7:10634–10640.
[26] Zhou Y, Gao B, Zimmerman AR, et al. Biochar-supported zerovalent iron reclaims silver from aqueous solution to form antimicrobial nanocomposite. Chemosphere. 2014;117:801–805.
[27] Yao Y, Gao B, Inyang M, et al. Removal of phosphate from aqueous solution by biochar derived from

anaerobically digested sugar beet tailings. J Hazard Mater. 2011;190:501.
[28] Yan J, Han L, Gao W, et al. Biochar supported nanoscale zerovalent iron composite used as persulfate activator for removing trichloroethylene. Bioresour Technol. 2015;175:269–274.
[29] Wang S, Gao B, Li Y, et al. Adsorptive removal of arsenate from aqueous solutions by biochar supported zero-valent iron nanocomposite: batch and continuous flow tests. J Hazard Mater. 2017;322:172–181.
[30] Yean S, Cong L, Yavuz CT, et al. Effect of magnetite particle size on adsorption and desorption of arsenite and arsenate. J Mater Res. 2005;20:3255–3264.
[31] Auffan M, Rose J, Proux O, et al. Enhanced adsorption of arsenic onto maghemites nanoparticles: As(III) as a probe of the surface structure and heterogeneity. Langmuir. 2008;24:3215–3222.
[32] Kappler A, Wuestner ML, Ruecker A, et al. Biochar as an electron shuttle between bacteria and Fe(III) minerals. Environ Sci Technol Lett 2014; 1:339-344.
[33] Dong X, Ma LQ, Gress J, et al. Enhanced Cr(VI) reduction and As(III) oxidation in ice phase: Important role of dissolved organic matter from biochar. J Hazard Mater. 2014;267:62–70.
[34] He F, Zhao D. Manipulating the size and dispersibility of zerovalent iron nanoparticles by use of carboxymethyl cellulose stabilizers. Environ Sci Technol. 2007;41:6216–6221.